Frontiers in Computing and Intelligent Systems
ISSN: 2832-6024 | Vol. 18, No. 2, 2026

Research on a Visual Reading Method for Pointer Instruments Integrating Geometric Constraints

Rui Song [1], Yimin Hou [2]

[1] Jilin University of Chemical Technology, Jilin City, Jilin Province, 132022, China
[2] Northeast Electric Power University, Jilin City, Jilin Province, 132012, China

Abstract: A pointer meter automatic reading algorithm integrating geometric constraints is proposed. First, the dial region is located by the Hough circle transform, and the dial centre is taken as the pointer rotation centre. Then, segmentation thresholds are selected adaptively according to the pointer colour, pointer pixels are extracted within a restricted annulus, and the pointer direction is determined by angular histogram voting. Next, the recognition result is screened for geometric consistency using the rotation centre, annulus and confidence constraints, and a rejection state is output when the evidence is insufficient. Finally, the meter reading is calculated from the angular proportion of the pointer between the start and end scale marks. A 0 to 6 bar pressure gauge in a public real-image dataset is taken as the object, and the accepted readings are established by two independent reading rounds and a third-round arbitration. The experimental results show that the mean absolute error of 10 test samples is 0.375 bar with a fiducial error of 6.24 percent; for the 8 samples whose pointer direction is correctly judged, the mean absolute error is 0.100 bar with a fiducial error of 1.66 percent; the recognition confidence of yellow pointers is clearly higher than that of dark and light pointers, so the rejection threshold should be set separately for each pointer colour.

Keywords: Pointer Meter; Machine Vision; Geometric Constraint; Hough Circle Transform; Automatic Reading.

1. Introduction

Pointer meters are widely used in electric power, chemical engineering, manufacturing, and other fields because of their simple structure, low cost, strong resistance to electromagnetic interference, and intuitive indication of changing trends. However, because their displayed values cannot be converted directly into electrical signal outputs, readings are generally taken manually on site. Reading is inefficient and easily affected by the viewing angle and the operator's condition when meters are mounted high, equipment is densely arranged, or periodic verification is required. With the widespread adoption of computer vision in industry, image-based automatic meter-reading methods have become increasingly common[1, 2].

Current methods for automatically reading pointer meters typically comprise meter localization, pointer recognition, and reading calculation. Meter localization mainly uses template registration or object detection. Sun et al.[3] used template registration and progressive localization to identify the meter region. This method is sensitive to meter type, shooting distance, and local texture; Howells et al.[4] implemented meter localization and real-time transcription on mobile devices, but focused primarily on inference speed under limited computing resources. In complex environments, Zhu et al.[5] reported that rain and fog simultaneously reduce the contrast of dial edges and fine scale marks, and that a single image-enhancement technique cannot eliminate all reading errors; Liu et al.[6] used multistage enhancement for low-quality outdoor images, but glass reflections, oblique projection, and local occlusion still alter the spatial relationship between the pointer and the scale. Pointer recognition methods mainly include attention networks and detection-segmentation approaches. Zhang et al.[7] introduced an attention mechanism to enhance locally salient regions, but this does not ensure that the pointer axis passes through the rotation centre; Deng et al.[8] combined object detection with semantic segmentation to read meters in UAV inspection images. Because each meter occupies only a small proportion of the image, pointer details are easily lost. Reading calculation methods mainly include angle-based and distance-based approaches. Xu et al.[9] used Deming regression and ROI refinement to fit the pointer line, improving reading accuracy; Leon-Alcazar et al.[10] trained a network on synthetic data and then calculated readings from real images, but differences remain between synthetic and field images.

Although these methods have achieved some success, limitations remain. For example, some require large-scale pixel-level or keypoint-annotated data to train their networks, while others do not constrain the geometric relationships among the pointer axis, the rotation centre, and the scale, causing incorrect readings to be output when the pointer is misidentified or the centre is offset. In addition, the source of the ground-truth readings used in some studies is unclear, reducing the credibility of error evaluation. These limitations weaken the adaptability and verifiability of the associated methods.

This paper proposes an automatic pointer-meter reading method that integrates geometric constraints. First, the dial is localized using the Hough circle transform, and the dial centre is taken as the pointer rotation centre. Next, pointer pixels are extracted adaptively according to pointer colour, and the pointer direction is determined by angular histogram voting. The recognition result is then screened using rotation-centre, annulus, and confidence constraints. Finally, the meter reading is calculated from the angular proportion of the pointer between the start and end scale marks. To ensure credible error evaluation, two independent reading rounds and a third-round adjudication are used to establish the manual readings. Experiments show that the method yields accurate readings when the pointer direction is correctly determined and can distinguish low-confidence results using the confidence measure.

2. Pointer-Meter Reading Algorithm

2.1. Meter-Region Localization

A two-stage method combining an object-detection network with a semantic-segmentation network can effectively localize a meter and extract its pointer[11, 12], while dial-segmentation studies in substation scenes also show that local structural features are important for scale-mark localization[13]. However, these methods require large amounts of annotated data. Because the outer edge of a circular pointer meter has a distinct circular shape, this paper uses the Hough circle transform to localize the dial and takes its centre as the pointer rotation centre. The circular region defined by this centre and the dial radius is used as the meter region for subsequent processing.

First, the image is converted to grayscale, and a 5 x 5 median filter is used to suppress the effect of noise on edge detection. The gradient Hough circle transform is then used to vote on edge points. Let the coordinates of an edge point in the image be (x, y), the candidate circle centre be (a, b), and the radius be r. Then

$$(x-a)^2+(y-b)^2=r^2, r_{\min}<r<r_{\max} \quad (1)$$

where a, b, and r accumulate votes in parameter space. The circle with the largest accumulator value is taken as the outer edge of the dial, with centre $C(c_x, c_y)$, and radius R; $r_{\min}$ and $r_{\max}$ are the radius thresholds used to exclude interference from adjacent meters and background arcs; they are set to 90 and 230 pixels, respectively. Research on adaptive recognition indicates that practical deployment should distinguish between detection-box quality and dial-geometry quality[14]; perspective correction can reduce distortion caused by oblique views but requires stable corresponding points[15]; input scaling in lightweight detection networks also changes the effective pixel width of fine scale marks[16]. Therefore, the meter region is cropped at the original resolution, and the unenhanced image is retained for subsequent review. The meter-region localization result is shown in Fig. 1(b).

2.2. Pointer Recognition

Based on the shape and colour characteristics of meter pointers, a method combining colour segmentation and angular histogram voting is proposed to localize the pointer and determine its direction. In terms of shape, the pointer consists of a slender shaft and a broad counterweight near the rotation centre, with the shaft tip extending toward the scale. In terms of colour, the pointer colour is fixed for a given meter and differs clearly from the dial background. Chen et al.[17] combined projection, thinning, and line-segment detection to recognize the pointer; keypoint methods[18, 19] and segmentation networks[20, 21] determine the pointer from the tip and centre keypoints or from a pixel-level mask, respectively. Both latter approaches require image-by-image annotation.

First, segmentation thresholds are selected according to pointer colour. Dark pointers are segmented in grayscale space, while light and yellow pointers are segmented in HSV space. The candidate pointer-pixel set Mis

$$M=(x,y)|g<T_g, \text{ for dark pointers; } (x,y)|V>T_V, S<T_S, \text{ for light pointers; } (x,y)|H_1<H<H_2, S>T_S', V>T_V', \text{ for yellow pointers} \quad (2)$$

where g is the grayscale value, H, S, V are the hue, saturation, and value, respectively, and T are the corresponding thresholds. In this study, the settings are $T_g=90, T_V=150, T_S=80, H_1=15, H_2=40, T_S'=T_V'=100$.

Next, to exclude interference from same-colour pixels belonging to the rotation-centre screw, scale numerals, and trademark graphics, only candidate pixels within the annulus on the inner side of the scale are retained, giving

$$M'=(x_i,y_i)\in M|\rho_{\text{in}}\cdot R<d_i<\rho_{\text{out}}\cdot R \quad (3)$$

where d_i is the distance from the pixel to centre C, and ρ_{in} and ρ_{out} are the inner and outer annulus-radius ratios. In this study, the inner ratio is set to $\rho_{\text{in}}=0.10$, the outer ratio for dark and yellow pointers is set to $\rho_{\text{out}}=0.80$, and the outer ratio for light pointers is set to $\rho_{\text{out}}=0.62$.

Finally, the angle of each pixel in M' relative to the centre is calculated as

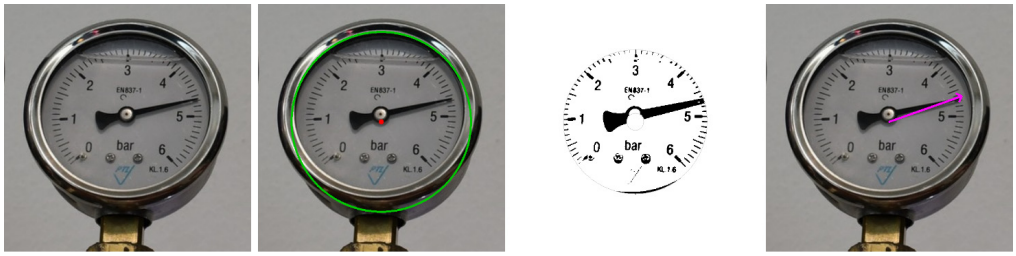
$$\theta_i=arctan2(x_i-c_x, c_y-y_i) \quad (4)$$

Angles are measured clockwise from 0 degrees at the 12 o'clock position. Because pixels at the far end of the pointer shaft more reliably indicate its direction, whereas the counterweight is concentrated near the centre, d_i is used as the weight to construct a 1-degree-resolution angular histogram, whose peak angle is θ_{peak}; pixels within the $\theta_{\text{peak}}\pm 8°$ window are then combined by weighted vector summation to obtain the pointer direction angle θ_p. This retains as much shaft information as possible while reducing the effect of the counterweight and same-colour interfering pixels. For dark pointers, the number of dark pixels may also be counted radially at each angle, with the direction containing the most pixels taken as the pointer direction. Both procedures are forms of angular voting. The pointer-recognition process is shown in Fig. 1.

2.3. Geometric-Consistency Constraints

Detection- and semantic-segmentation-based reading methods can provide a reference for mask extraction[22], while structural enhancement and keypoint constraints can improve robustness in complex environments[23]. This paper uses geometric-consistency constraints to determine whether a recognition result is reliable. The confidence of the angle estimate is defined as

$$c=\frac{\Sigma_{i\in W} d_i}{\Sigma_{i\in M'} d_i} \quad (5)$$



(a) Original image (b) Dial localization (c) Pointer extraction (d) Pointer direction

Fig 1. Pointer-recognition process

where W is the set of pixels within the peak window. As c increases, the candidate pixels in the annulus become more concentrated in one direction, providing stronger geometric evidence for the pointer direction; as c decreases, a larger proportion of the pixels are interference from scale numerals, screws, or reflections. A rejection state is output if any of the following occurs: no dial circle satisfying the radius threshold is detected; fewer than 20 pointer-candidate pixels are found in the annulus; the confidence c is below the threshold T_c; or the pointer direction angle lies outside the valid arc bounded by the start and end scale angles. Although lightweight segmentation can accelerate mask extraction, it cannot replace range validation and outlier blocking[24]. Therefore, these constraints must be retained regardless of the segmentation method used.

2.4. Meter-Reading Calculation

The meter reading is calculated from the pointer direction angle and the start and end major scale marks, which determine the value corresponding to the pointer's relative position within the valid arc. Equation (6) gives the reading formula, in which $\hat{v}$ denotes the calculated meter reading.

$$\hat{v} = \frac{\theta_p - \alpha}{\beta - \alpha} \times (v_1 - v_0) + v_0 \tag{6}$$

where α, β are the angles of the start and end major scale marks, respectively, and v_0, v_1 are the corresponding scale values. All angles are unwrapped clockwise into the same continuous interval. If the scale intervals are unequal, the two adjacent major scale marks bracketing the pointer replace the start and end marks, and Eq. (6) is used for interpolation within the local interval[25]. For a pointer-angle error of $\Delta\theta$, the reading error is

$$\Delta v = \frac{(v_1 - v_0)}{(\beta - \alpha)} \times \Delta\theta \tag{7}$$

Equation (7) shows that a larger measurement range and a smaller valid-arc angle produce a greater reading error for a given angular error. The theoretical angular sensitivities of the five meter types are shown in Table 2. This table illustrates only how measurement range and arc angle affect error propagation; it does not represent the measured error of the algorithm.

3. Experimental Analysis

3.1. Experimental Data and Platform

The experimental material is limited to available, verifiable public real-image data. The tasks and annotation status of each dataset are shown in Table 1. Scene isolation and cross-set deduplication have been verified by shooting session for the PaddleX detection and segmentation sets. The detection set contains 783 images and the segmentation set 407 images; both are reserved for subsequent network training. The reading experiment uses the pointer-meter-reader dataset, which contains 40 photographs divided into 31 groups according to the release-package directory, with five meter types in each photograph. The group-level values supplied with the release package lack independent calibration or per-image measurement evidence and are therefore not used as ground-truth readings. Unlike the 213 real images of 15 pressure gauges used by Zuo et al.[26], the present reading experiment has a smaller sample size, and its conclusions apply only to the selected meter. Networks such as lightweight YOLO, U²-Net, and LinkNet[27, 28] can improve localization and segmentation accuracy but require large annotated datasets, so they are not used in this study.

Table 1. Datasets and annotation status

Dataset	Task	Number of images	Annotation status
PaddleX detection set	Dial detection	783 images: 464 training, 30 validation, and 289 test	Meter bounding boxes
PaddleX segmentation set	Pointer and scale segmentation	407 images: 259 training, 24 validation, and 124 test	Pixel-level masks
pointer-meter-reader	Reading experiment	40 photographs in 31 groups	Group-level values, not used as ground-truth readings

Table 2. Theoretical angular sensitivity of different meters

Meter	Range width	Valid-arc angle	Reading change per degree	Reading error for a 2-degree angular error
Meter 1	1.6 bar	275.5°	0.0058 bar	0.0116 bar
Meter 2	6 bar	271.4°	0.0221 bar	0.0442 bar
Meter 3	160 psi	239.8°	0.6672 psi	1.3344 psi
Meter 4	10 bar	275.5°	0.0363 bar	0.0726 bar
Meter 5	120 ℃	270.1°	0.4443 ℃	0.8886 ℃

The reading experiment uses the circular, single-pointer pressure gauge with a range of 0-6 bar and a minimum division of 0.1 bar, namely Meter 2 in the table. One photograph with a complete dial is selected from each group, giving 31 photographs in total. The 21 photographs in Groups 1-21 are development samples used to adjust parameters such as the candidate region for the circle centre. The 10 photographs in Groups 22-31 are test samples; automatic readings are obtained in a single run after the parameters are frozen, with no further adjustment. The pointer-colour confidence analysis additionally uses eight photographs each of Meters 2, 3, and 4, plus eight repeated photographs of Meter 5, for a total of 32 photographs. Python is used as the development language and OpenCV as the computer-vision library.

3.2. Acquisition of Manual Readings

To obtain reliable manual readings, the 31 samples are interpreted in three rounds. In the first round, a multimodal large language model reads each enlarged dial image. In the second round, a human reader independently interprets the images. Both rounds record the reading, uncertainty range, and rationale, and neither reader knows the other's result. After the second-round records are standardized to common

units and checked for row order, the results are merged according to

$$v_{\text{ref}} = \frac{v^{(1)}+v^{(2)}}{2}, \quad \left|v^{(1)} - v^{(2)}\right| \le u^{(1)} + u^{(2)} \qquad (8)$$

where $v^{(1)}$, $v^{(2)}$ are the readings from the two rounds, and $u^{(1)}$, $u^{(2)}$ are the uncertainty ranges reported in the two rounds. Samples that do not satisfy Eq. (8), as well as samples lacking a valid second-round record, are submitted to a third independent reader for adjudication, with the adjudicated value taken as the accepted reading. The merged results are as follows: the two readings agree for 24 samples, differ by more than the uncertainty range for 6 samples, and the second-round record is invalid for 1 sample. The latter 7 samples are all adjudicated in the third round. The uncertainty range reported in the third round is ±1 bar, and no rationale is recorded; consequently, these readings have lower confidence than the first 24.

3.3. Experimental Results and Analysis

3.3.1. Reading Accuracy

To evaluate the accuracy of the proposed algorithm, the automatic readings of the 10 test samples are compared with the accepted readings. The ratio of the absolute error to the measurement range is used as the fiducial error. The results are shown in Table 3.

Table 3. Reading results (readings in bar; fiducial error in %)

No.	Sample	Round 1 reading	Round 2 reading	Accepted reading	Automatic reading	Absolute error	Fiducial error
1	setup22	4.45	4.30	4.375	4.433	0.058	0.97
2	setup23	0.40	0.50	0.450	0.378	0.072	1.20
3	setup24	2.55	2.60	2.575	3.844	1.269	21.15
4	setup25	5.75	5.70	5.725	4.044	1.681	28.02
5	setup26	4.65	4.60	4.625	4.578	0.047	0.78
6	setup27	3.95	3.90	3.925	3.900	0.025	0.42
7	setup28	2.95	2.40	2.300	2.089	0.211	3.52
8	setup29	1.75	1.70	1.725	1.756	0.031	0.52
9	setup30	0.95	0.90	0.925	0.700	0.225	3.75
10	setup31	3.00	2.70	2.850	2.722	0.128	2.13

Table 3 shows that the mean absolute error of the 10 test samples is 0.375 bar and the mean fiducial error is 6.24%. Samples 3 and 4 have markedly larger errors, with absolute errors of 1.269 bar and 1.681 bar, respectively. Review of the overlay images shows that in both cases the detected dial centre is shifted to the upper right of the true rotation centre, causing the output pointer direction to be opposite to the actual direction. After excluding these two samples with incorrect direction determination, the remaining eight samples have a mean absolute error of 0.100 bar, a mean fiducial error of 1.66%, and a maximum absolute error of 0.225 bar, corresponding to a fiducial error of 3.75%. The direction-determination accuracy is 80%. As shown in Table 2, the reading of Meter 2 changes by approximately 0.022 bar per degree. A mean absolute error of 0.100 bar therefore corresponds to an angular error of approximately 4.5 degrees, indicating that when the direction is correctly determined, the reading error mainly arises from centre offset and pointer-axis fitting error. In addition, the accepted reading for Sample 7 comes from the third-round adjudication and has a wider uncertainty range, so the reliability of its 0.211 bar error is lower than that of the other samples.

3.3.2. Effect of Pointer Colour on Recognition Confidence

To analyse the effect of pointer colour on the reliability of angle estimation, the confidence values of 32 photographs are calculated using Eq. (5), and a common threshold of 0.15 is used to classify results as accepted or rejected. The results are shown in Table 4.

Table 4. Confidence and rejection results for pointer-colour branches

Pointer colour	Meter	Mean confidence	Confidence range	Rejected samples
Dark	Meter 2	0.131	0.072-0.202	6/8
Dark	Meter 5	0.130	0.113-0.179	6/8
Light	Meter 4	0.224	0.148-0.252	3/8
Yellow	Meter 3	0.966	0.962-0.970	0/8

Table 4 shows that yellow pointers contrast strongly against red and black dial backgrounds, producing a mean confidence of 0.966; all eight photographs are accepted. The mean confidence values of dark and light pointers are only 0.13-0.22, mainly because of same-colour numerals, screws, and reflected pixels on the dial. Applying the same absolute threshold as for yellow pointers would therefore cause many false rejections. Thus, the confidence defined in Eq. (5) is closely related to pointer colour. Rejection thresholds should not be set uniformly across colours; instead, they should be calibrated separately for each colour or based on within-colour quantiles.

3.3.3. Analysis of Failure Samples

Research on aircraft-instrument recognition separates image-shake removal, centre detection, and pointer localization into independent stages, making it easier to identify the source of error [29]. Following this approach, the errors in the two failure samples in this study both occur during meter-region localization. The Hough circle transform detects the metal outer rim of the dial. When the viewing angle is oblique or reflections from the outer rim are uneven, the centre of the outer rim no longer coincides with the pointer rotation centre. In Fig. 1(b), the detected centre is also slightly below the rotation axis; a larger offset causes the pointer direction to be misidentified. Moreover, the test program outputs readings for all 10 samples without triggering rejection, showing that pixel-count and radius thresholds alone are insufficient to detect centre offsets. Research on human-like reading sequences suggests that identifying the scale interval before locating the pointer tip can reduce the ambiguity of relying on a global angle alone[30]. Future work can introduce networks such as lightweight YOLO, U²-Net, and LinkNet[27, 28] to detect the rotation centre and scale points, and can validate the centre using a co-circularity constraint on the scale marks so that a rejection state is output when the centre is offset. All failure samples are retained in the test records; none are removed or used for retrospective

parameter tuning because of unfavourable results.

4. Conclusion

Using a circular, single-pointer pressure gauge as an example, this paper develops an automatic reading algorithm that integrates geometric constraints. The dial is first localized with the Hough circle transform to determine the pointer rotation centre. Pointer pixels are then extracted adaptively according to pointer colour, and the pointer direction is determined by combining an annulus constraint with angular histogram voting. The recognition result is subsequently screened using confidence and valid-arc constraints. Finally, the meter reading is calculated from the angular proportion of the pointer between the start and end scale marks. To ensure credible error evaluation, accepted readings are established using two independent reading rounds and a third-round adjudication. Experiments show that the 10 test samples have a mean absolute error of 0.375 bar and a fiducial error of 6.24%; the eight samples whose directions are correctly determined have a mean absolute error of 0.100 bar and a fiducial error of 1.66%. The experiments also show that the recognition confidence of yellow pointers is substantially higher than that of dark and light pointers, so rejection thresholds should be set separately by pointer colour. The limitations of this study are that the reading experiment covers only one meter type and uses a small test set, the accepted readings for seven samples come from third-round adjudication, and the method cannot yet reject results automatically when the dial centre is offset. Future work will introduce deep networks to detect the rotation centre and scale points and will repeat the reading procedure on the remaining meters to evaluate the method's generalizability.

References

[1] Li, J., Yuan, L., & Ran, T. (2021). Automatic detection and reading method for pointer meters based on YOLOv4. Mechanical & Electrical Engineering, 38(7), 912–917. (in Chinese)

[2] Dong, Z., Gao, Y., Yan, Y., et al. (2021). Vector Detection Network: An Application Study on Robots Reading Analog Meters in the Wild. IEEE Transactions on Artificial Intelligence, 2(5), 394–403. https://doi.org/10.1109/TAI.2021.3107050.

[3] Sun, X., Hou, L., & Qu, H. (2021). Progressive automatic reading method for pointer meters based on convolutional neural networks. Chinese Journal of Sensors and Actuators, 34(10), 1326–1333. (in Chinese)

[4] Howells, B., Charles, J., & Cipolla, R. (2021). Real-Time Analogue Gauge Transcription on Mobile Phone. In Proceedings of the IEEE/CVF Conference on Computer Vision and Pattern Recognition Workshops (pp. 2369–2377). https://doi.org/10.1109/CVPRW53098.2021.00274.

[5] Zhu, B., & Fan, S. (2021). Recognition method for pointer meters in substations under rainy and foggy conditions. Laser & Optoelectronics Progress, 58(24), 2410008. (in Chinese)

[6] Liu, M., Wang, B., Luo, P., et al. (2024). Intelligent recognition method for pointer-meter readings in low-quality outdoor images. High Voltage Engineering, 50(11), 5034–5046. (in Chinese)

[7] Zhang, S., Wan, J., Wang, H., et al. (2022). Image-reading recognition method for pointer meters based on an attention-enabled convolutional neural network. Electric Power Automation Equipment, 42(4), 218–224. (in Chinese)

[8] Deng, G., Huang, T., Lin, B., et al. (2022). Automatic Meter Reading from UAV Inspection Photos in the Substation by Combining YOLOv5s and DeeplabV3+. Sensors, 22(18), 7090. https://doi.org/10.3390/s22187090.

[9] Xu, X., Chen, X., & Mao, Y. (2023). Pointer-meter reading technology based on Deming regression and ROI refinement. Journal of Jiangsu University (Natural Science Edition), 44(3), 324–329. (in Chinese)

[10] Leon-Alcazar, J., Alnumay, Y., Zheng, C., et al. (2024). Learning to Read Analog Gauges from Synthetic Data. In Proceedings of the IEEE/CVF Winter Conference on Applications of Computer Vision (pp. 8616–8625). https://doi.org/10.1109/WACV57701.2024.00854.

[11] Jin, A., Yuan, L., Zhou, D., et al. (2022). Pointer-meter reading recognition method based on YOLOv5 and U-Net. Instrument Technique and Sensor, (11), 29–33. (in Chinese)

[12] Zou, L., Wang, K., Wang, X., et al. (2023). Automatic Recognition Reading Method of Pointer Meter Based on YOLOv5-MR Model. Sensors, 23(14), 6644. https://doi.org/10.3390/s23146644.

[13] Huang, S., Fan, S., & Wang, Z. (2022). Pointer-meter reading recognition method for substations based on CenterNet and DeepLabv3+. Journal of Electric Power, 37(3), 232–243. (in Chinese)

[14] Zhao, W., Chen, H., Guo, L., et al. (2023). Adaptive recognition method for substation meter readings based on YOLO-E and improved OCRNet image segmentation. Electric Power Construction, 44(11), 75–85. (in Chinese)

[15] Tan, L., Wu, W., Ding, J., et al. (2024). A Robust Pointer Meter Reading Recognition Method Based on TransUNet and Perspective Transformation Correction. Electronics, 13(13), 2436. https://doi.org/10.3390/electronics13132436.

[16] Liu, Y., Li, Y., Zhang, T., et al. (2023). Pointer-meter detection and reading recognition based on improved YOLOv5s. Journal of Beijing Information Science and Technology University (Natural Science Edition), 38(3), 9–14. (in Chinese)

[17] Chen, C., Wang, Q., & Yao, W. (2022). Automatic reading algorithm for pointer meters based on machine vision. Transducer and Microsystem Technologies, 41(10), 130–133. (in Chinese)

[18] Tao, J., Lin, W., Zeng, L., et al. (2023). Pointer-meter reading recognition based on YOLOv4-tiny and Hourglass. Journal of Electronic Measurement and Instrumentation, 37(5), 1–10. (in Chinese)

[19] Gong, Q., Bie, B., Fan, X., et al. (2023). Pointer-meter reading algorithm based on keypoint detection. Journal of Electronic Measurement and Instrumentation, 37(3), 66–73. (in Chinese)

[20] Liu, Y., Tusongjiang Kari, Yilihamu Yarmaimaiti, et al. (2024). Fully automatic pointer-meter reading method based on VCA-UNet. Instrument Technique and Sensor, (2), 36–43. (in Chinese)

[21] Wang, J., Zhang, S., Wang, X., et al. (2025). Meter-reading recognition based on improved U2Net. Microelectronics & Computer, 42(7), 93–102. (in Chinese)

[22] Hou, L., Wang, S., Sun, X., et al. (2023). A pointer meter reading recognition method based on YOLOX and semantic segmentation technology. Measurement, 218, 113241. https://doi.org/10.1016/j.measurement.2023.113241.

[23] Wang, J., Zeng, J., Kang, B., et al. (2025). A Keypoint-Driven Robust Pointer Meter Reading Method With Enhanced Structure for Complex Environments. IEEE Transactions on Instrumentation and Measurement, 74, 1–16. https://doi.org/10.1109/TIM.2025.3464414.

[24] Yan, F., Xu, W., Huang, Q., et al. (2022). Fully automatic recognition of pointer-meter readings based on a lightweight semantic-segmentation model. Laser & Optoelectronics Progress, 59(24), 2410001. (in Chinese)

[25] Qu, H., & Zhang, W. (2023). Pointer-meter detection and recognition based on YOLOv7+U2-Net. Computer Systems & Applications, 32(11), 276–285. (in Chinese)

[26] Zuo, Z., Li, Y., Chen, L., et al. (2024). Automatic pointer-meter reading method based on machine vision. Instrument Technique and Sensor, (6), 37–40. (in Chinese)

[27] Su, Y., Si, H., Tang, X., et al. (2025). Intelligent reading method for pointer meters based on lightweight YOLOv5s and U²-Net. Journal of Jishou University (Natural Sciences Edition), 46(4), 44–51. (in Chinese)

[28] Lu, X., Zhu, S., & Lu, B. (2024). Pointer Meter Reading Method Based on YOLOv8 and Improved LinkNet. Sensors, 24(16), 5288. https://doi.org/10.3390/s24165288.

[29] Lin, K., & Han, F. (2025). Automatic recognition of aircraft-instrument information based on image processing and computer vision. Automation & Instrumentation, (8), 78–82. (in Chinese)

[30] Liu, Q., & Shi, L. (2025). A pointer meter reading method based on human-like reading sequence and keypoint detection. Measurement, 248, 116994. https://doi.org/10.1016/j.measurement.2025.116994.